IEEE Access
Multidisciplinary | Rapid Review | Open Access Journal

Received 13 June 2024, accepted 2 July 2024, date of publication 4 July 2024, date of current version 12 July 2024.

Digital Object Identifier 10.1109/ACCESS.2024.3423355

RESEARCH ARTICLE

A Novel Method for the Computation of the Deterministic Maximum Likelihood Estimator of Multiple Real Sinusoids

PASQUALE DI VIESTI[1], (Graduate Student Member, IEEE), JESUS SELVA[2], AND GIORGIO M. VITETTA[1], (Senior Member, IEEE)

[1]Department of Engineering "Enzo Ferrari" (DIEF), University of Modena and Reggio Emilia, 41125 Modena, Italy
[2]Department of Physics, Systems Engineering and Signal Theory (DFISTS), University of Alicante, 03080 Alicante, Spain

Corresponding author: Pasquale Di Viesti (pasquale.diviesti@unimore.it)

This work was supported by the Spanish Ministry of Science and Innovation under Project PID2020-117303GB-C22.

ABSTRACT In this manuscript a novel computationally efficient method for implementing the Deterministic Maximum Likelihood estimator of multiple superimposed real sinusoids is derived. This method is an adaptation of a recently proposed algorithm for the estimation of undamped exponentials and offers two significant advantages in terms of complexity with respect to various alternatives available in the technical literature. First, the dependence of the computational complexity on the snapshot length is the same as that of the Fast Fourier Transform. Consequently, increasing the snapshot length does not have a substantial impact on the overall computational burden. Second, the proposed method exploits the ability of the periodogram estimator to coarsely locate the global maximum of the Deterministic Maximum Likelihood cost function, thereby eliminating the need for a global search on this last function. Our numerical results show that it achieves a better accuracy-complexity trade-off than various estimators available in the literature.

INDEX TERMS Amplitude estimation, array signal processing, direction-of-arrival estimation, discrete Fourier transforms, Fourier transforms, frequency estimation, harmonic analysis, interpolation, maximum likelihood estimation, parameter estimation.

I. INTRODUCTION

The estimation of the parameters of multiple sinusoids, especially their frequencies, is one of the oldest problems in signal processing and is a fundamental problem in various fields, including radar systems and wireless communications [1], [2], [3], [4], [5]. Most of the solutions available in the technical literature employ a procedure consisting of the following three steps. First, the so-called periodogram of the set of measured samples (also termed *snapshot*) is computed, which consists of the *Fast Fourier Transform* (FFT) of these samples followed by the computation of their square absolute value. Second, the main local maxima of the periodogram are located and their corresponding abscissas are taken as the initial coarse estimates of the frequencies. And third, these estimates are improved through either interpolation formulas or an iterative algorithm to obtain the final frequency estimates. This standard procedure has been followed in many papers, such as [6], [7], [8], [9], and [10], and although its first two steps are computationally efficient, they have two fundamental shortcomings. First, the procedure may fail to estimate closely spaced frequencies or produce biased estimates when the separation is small [11], [12], [13]. Second, the third step requires periodogram samples at off-grid frequencies. Unluckily, the computational cost required for this task is substantial, usually of order $\mathcal{O}(N)$ where N is the snapshot length.

In the literature, various attempts have been made to mitigate the first shortcoming by adapting estimators originally designed for *direction of arrival* (DOA) estimation, such as *multiple signal classification* (MUSIC), *estimation of signal parameters via rotational invariant techniques* (ESPRIT),

The associate editor coordinating the review of this manuscript and approving it for publication was Gerard-Andre Capolino.

Newtonalized orthogonal matching pursuit (NOMP) [14], various implementations of the *Deterministic Maximum Likelihood* (DML) estimator [15], [16], [17] and methods based on the variational Bayesian inference method [18], [19]. However, this approach is problematic for two reasons. First, frequency estimation is typically performed on the basis of a single snapshot, whereas most DOA estimators require multiple snapshots [20], [21]. Second, the snapshot length N is usually large in frequency estimation, but small in DOA estimation. As DOA estimators involve a large number of $\mathcal{O}(N)$ operations, their adaptation to the multiple frequency estimation problem usually entails a significant computational burden. For this reason, more recently, Fourier-based methods have been proposed in [22], [23], [24], [25], and [26].

An alternative approach, circumventing the previous two shortcomings and exploiting the favorable interpolation properties of trigonometric polynomials, has been presented in a series of papers [27], [28], [29]. In these manuscripts it was shown that the DML estimate of multiple frequencies can be computed with a complexity independent of the snapshot length N, once the output of the initial FFT is available. This is due to the fact that the correlations required to compute DML estimates through complicated procedures, such as the *Alternate Projection* (AP) method in [16] or the Newton method in [27], can be obtained either through closed-form formulas or through accurate interpolation methods requiring a few FFT samples only. From a complexity perspective, this result implies that no $\mathcal{O}(N)$ operation is required, so that excellent estimators, such as the DML estimator, can be implemented with low computational burden.

Multiple frequency estimation can be performed for two related cases, one involving the superposition of multiple real sinusoids and another involving multiple undamped exponentials. If we refer to these two variants as real and complex *multiple frequency* (MF) problems, respectively, the results in [2], [3], [27], [28], [29], [31], and [32] apply only to the complex MF problem. The purpose of this paper is to show how various mathematical results illustrated in the above-mentioned references can be applied to the real MF problem without any mismatch or performance degradation. This leads to the development of an estimation method that can be viewed as the real counterpart of the methods illustrated in [2], [3], [27], [28], and [29]. For this reason, this method can evaluate DML estimates in the real MF problem with N-independent complexity, once the initial FFT is computed.

The remainder of this paper is organized as follows. In Section II, we briefly recall the complex MF problem and the computational procedure required for the DML estimator. In Section III, a new signal model is proposed for the real MF problem and the related ML cost function is presented. Section IV presents a new method for the efficient computation of the real DML multiple-frequency estimates. The performance of our estimator is compared with that of other estimators available in the literature in Section V. Finally, conclusions are presented in Section VI.

A. NOTATION

The following notation is adopted throughout the paper:

1) Vectors are written in bold face (e.g., $\mathbf{x}$) and are always assumed to be column vectors. The matrices are written in upper bold face (e.g., $\mathbf{X}$).
2) $[\mathbf{x}]_n$ denotes the nth element of the vector $\mathbf{x}$.
3) $[\mathbf{X}]_{m,n}$ denotes the (m, n)th element of the matrix $\mathbf{X}$.
4) For any column vector $\mathbf{y}$ of length N, $\mathbf{y}^{(d)}$ denotes the $2N \times 1$ vector generated by duplicating all components of $\mathbf{y}$, so that
$$[\mathbf{y}^{(d)}]_{2n-1} = [\mathbf{y}^{(d)}]_{2n} \triangleq [\mathbf{y}]_n, \tag{1}$$
with $n = 1, 2, \ldots, N$.
5) The sub-scripts $(\cdot)_R$ and $(\cdot)_I$ denote the real and imaginary parts, respectively. Thus, for example, for a complex function $c(f)$, we have that $c_R(f) = \mathrm{Re}\{c(f)\}$ and $c_I(f) = \mathrm{Im}\{c(f)\}$.
6) $\mathbf{I}_N$ denotes the $N \times N$ identity matrix.
7) $[\mathbf{x}; \mathbf{y}]$ denotes the vertical concatenation of two column vectors $\mathbf{x}$ and $\mathbf{y}$.
8) $\mathbf{X}^\dagger$ is the Moore-Penrose pseudo-inverse of matrix $\mathbf{X}$. For any full column-rank matrix $\mathbf{X}$, it is given by
$$\mathbf{X}^\dagger = (\mathbf{X}^H\mathbf{X})^{-1}\mathbf{X}^H. \tag{2}$$
9) $\mathcal{R}(\mathbf{A}, \mathbf{B}) \triangleq \mathbf{A}^T\mathbf{B}$ denotes the correlation between the real matrices $\mathbf{A}$ and $\mathbf{B}$ of proper size.

II. COMPUTATION OF DML ESTIMATES FOR THE COMPLEX MF PROBLEM THROUGH THE PERIODOGRAM-NEWTON METHOD

In this section, we briefly recall the DML estimation problem considered in [2], [3], [27], [28], and [29] and the related signal model, both designed for the complex MF case. This problem involves the complex signal
$$x_c(t) \triangleq \sum_{k=1}^{K} a_{c,k} e^{j2\pi\nu_k t} + w_c(t), \tag{3}$$
that consists of a weighted sum of K undamped exponentials overlapped with noise; here, $a_{c,k}$ and ν_k represent the unknown complex amplitude and frequency, respectively, of the kth exponential, and $w_c(t)$ is a band-limited complex Gaussian noise process having zero mean. If the estimator samples the signal $x_c(t)$ at the instants $\{(n-1)T; 1 \le n \le N\}$ with sampling period T, the vector collecting the resulting samples can be written as
$$\mathbf{x}_c = \mathbf{V}_c(\mathbf{f})\mathbf{a}_c + \mathbf{w}_c, \tag{4}$$
where
$$[\mathbf{x}_c]_n \triangleq x_c((n-1)T), \quad [\mathbf{V}_c(\mathbf{f})]_{n,k} \triangleq e^{j2\pi f_k(n-1)},$$
$$[\mathbf{a}_c]_k \triangleq a_{c,k}, \quad [\mathbf{f}]_k \triangleq f_k \triangleq \nu_k T, \quad [\mathbf{w}_c]_n \triangleq \mathbf{w}_c((n-1)T), \tag{5}$$

with $n = 1, 2, \ldots, N$ and $k = 1, 2, \ldots, K$. If the elements of the Gaussian vector $\mathbf{w}_c$ are independent and identically distributed (i.i.d.), the DML estimate is the pair $(\hat{\mathbf{f}}, \hat{\mathbf{a}}_c)$ maximizing the cost function

$$L_{\mathrm{DML}}(\tilde{\mathbf{f}}, \mathbf{a}_c; \mathbf{x}_c) \triangleq -\|\mathbf{x}_c - \mathbf{V}_c(\tilde{\mathbf{f}})\tilde{\mathbf{a}}_c\|^2, \tag{6}$$

where $\tilde{\mathbf{f}}$ and $\tilde{\mathbf{a}}_c$ denote the trial values of $\mathbf{f}$ and $\mathbf{a}_c$ of size $K \times 1$. This optimization problem can be simplified by maximizing (6) in closed form with respect to $\tilde{\mathbf{a}}$ for a given $\tilde{\mathbf{f}}$. In fact, the global maximum of (6) in $\tilde{\mathbf{a}}_c$ for fixed $\tilde{\mathbf{f}}$ is attained at

$$\tilde{\mathbf{a}}_c = \mathbf{V}_c^{\dagger}(\tilde{\mathbf{f}})\mathbf{x}_c. \tag{7}$$

Thus, substituting this $\tilde{\mathbf{a}}_c$ into (6), produces the concentrated cost function

$$\bar{L}_c(\tilde{\mathbf{f}}; \mathbf{x}_c) = -\|\mathbf{x}_c - \mathbf{P}_c(\tilde{\mathbf{f}})\mathbf{x}_c\|^2, \tag{8}$$

where

$$\mathbf{P}_c(\tilde{\mathbf{f}}) \triangleq \mathbf{V}_c(\tilde{\mathbf{f}})\mathbf{V}_c(\tilde{\mathbf{f}})^{\dagger} \tag{9}$$

is the *orthogonal projection matrix* of $\mathbf{V}_c(\tilde{\mathbf{f}})$. Finally, note that maximizing the concentrated cost function $\bar{L}_c(\tilde{\mathbf{f}}; \mathbf{x}_c)$ (8) is equivalent to maximizing

$$L_c(\tilde{\mathbf{f}}; \mathbf{x}_c) \triangleq \mathbf{x}_c^H \mathbf{P}_c(\tilde{\mathbf{f}})\mathbf{x}_c, \tag{10}$$

given that $\mathbf{P}_c(\tilde{\mathbf{f}})$ is idempotent,[1] i.e., $\mathbf{P}_c(\tilde{\mathbf{f}})^2 = \mathbf{P}_c(\tilde{\mathbf{f}})$.

A method for maximizing $L_{\mathrm{DML}}(\tilde{\mathbf{f}}; \tilde{\mathbf{a}}_c, \mathbf{x}_c)$ (6), which results from combining the AP method in [16] with a Newton-type method, was proposed in [27], [28], and [29]. The main steps of this method, dubbed *Periodogram-Newton* (PN) method, are listed below.

Step 1) We sample $L_c(\tilde{f}; \mathbf{x}_c)$ (10) on a regular grid formed by bN samples, where $b > 1$ is an integer oversampling factor, i.e., we compute

$$L_c\left(\frac{p}{bN}; \mathbf{x}_c\right), \ p = 0, 1, \ldots, bN - 1. \tag{11}$$

Since $\mathbf{V}_c(\tilde{f})^H \mathbf{V}_c(\tilde{f}) = N$ ($\tilde{f}$ is a scalar), we have from (2) and (9) that the set of samples in (11) is just the length-(bN) periodogram of $\mathbf{x}_c$, which can be computed efficiently using an FFT. More precisely, since the periodogram of $\mathbf{x}_c$ is defined by

$$[\mathcal{P}_c(\mathbf{x}_c)]_{p+1} \triangleq \frac{1}{N}\left|[\mathbf{x}_{c,F}]_{p+1}\right|^2, \tag{12}$$

where $\mathbf{x}_{c,F}$ is the bN-length DFT of $\mathbf{x}_c$,

$$[\mathbf{x}_{c,F}]_{p+1} \triangleq \sum_{n=0}^{N-1} [\mathbf{x}_c]_{n+1} e^{-j2\pi pn/(bN)}, \tag{13}$$

it holds that

$$L_c\left(\frac{p}{bN}; \mathbf{x}_c\right) = [\mathcal{P}_c(\mathbf{x}_c)]_{p+1}. \tag{14}$$

[1]This property follows from the fact that $\mathbf{P}_c(\tilde{\mathbf{f}})$ is an orthogonal projection matrix.

Step 2) If the frequencies contained in the sequence $\mathbf{x}_c$ are close to the abscissas of the periodogram and the associated amplitudes are sufficiently above the noise level, they can be estimated with reasonable quality. Therefore, if we fix a detection threshold[2] ϵ and then form the set $\mathcal{I}$ of indices p such that $[\mathcal{P}_c(\mathbf{x}_c)]_{p+1} > \epsilon$, the above mentioned frequencies must be close to one of the frequencies $p/(bN)$, with p in $\mathcal{I}$. In this step, we compute the set $\mathcal{I}$ in preparation for steps 3) and 5) in which we require to scan either the periodogram $\mathcal{P}_c(\mathbf{x}_c)$ or a residual periodogram (defined in Step 5)) over the whole set of indices p, $0 \le p < bN - 1$. In those two steps, we scan over the set $\mathcal{I}$ rather than over the whole set p, $0 \le p < bN - 1$, thus reducing the complexity from $\mathcal{O}(N)$ to $\mathcal{O}(K)$.

Step 3) In this step, we determine the values of the index p in $\mathcal{I}$ for which $[\mathcal{P}_c(\mathbf{x}_c)]_{p+1}$ is a local maximum of the periodogram $\mathcal{P}_c(\mathbf{x}_c)$. The frequencies corresponding to each local maximum are then collected in the vector $\hat{\mathbf{f}}_0$. Note that this vector represents the coarse initial estimate of the set of frequencies contained in the sequence $\mathbf{x}_c$.

Step 4) The fourth step improves the initial estimate $\hat{\mathbf{f}}_0$ through an iterative Newton-type method. More specifically, if $\hat{\mathbf{f}}_\alpha$ (with $\alpha = 0, 1, \ldots, N_{\mathrm{it}} - 1$, where N_{it} denotes the maximum number of iterations) represents the vector of frequency estimates at the input of the αth iteration, the new estimate of $\mathbf{f}$ (i.e., $\hat{\mathbf{f}}_{\alpha+1}$) is computed following this two-step procedure:

1) Compute a new estimate of $\mathbf{a}_c$ given $\hat{\mathbf{f}}_\alpha$ as (see (7))

$$\hat{\mathbf{a}}_{c,\alpha} = \mathbf{V}_c(\hat{\mathbf{f}}_\alpha)^{\dagger}\mathbf{x}_c. \tag{15}$$

2) Compute a new estimate $\hat{\mathbf{f}}_{\alpha+1}$ of $\mathbf{f}$, given $\hat{\mathbf{a}}_{c,\alpha}$ and $\hat{\mathbf{f}}_\alpha$, as

$$\hat{\mathbf{f}}_{\alpha+1} = \hat{\mathbf{f}}_\alpha - \mu \mathbf{H}_c^{-1}(\hat{\mathbf{f}}_\alpha, \hat{\mathbf{a}}_{c,\alpha})\, \mathbf{g}_c(\hat{\mathbf{f}}_\alpha, \hat{\mathbf{a}}_{c,\alpha}), \tag{16}$$

where μ is a real positive parameter (step size),

$$\mathbf{g}_c(\mathbf{f}, \mathbf{a}_c) \triangleq 2\,\mathrm{Re}\{\mathbf{a}_c^* \odot (\mathbf{V}_{c,1}^H(\mathbf{x}_c - \mathbf{V}_c\mathbf{a}_c))\}, \tag{17}$$

and

$$\begin{aligned}\mathbf{H}_c(\mathbf{f}, \mathbf{a}_c) \triangleq 2\,\mathrm{Re}\{&(\mathbf{a}_c\mathbf{a}_c^H) \odot (\mathbf{V}_{c,1}^H\mathbf{V}_{c,1})^T \\ &- \mathrm{diag}\{\mathbf{a}_c^* \odot (\mathbf{V}_{c,2}^H(\mathbf{x}_c - \mathbf{V}_c\mathbf{a}_c))\}\}\end{aligned} \tag{18}$$

are the gradient and Hessian,[3] respectively, of $L_{\mathrm{DML}}(\mathbf{f}, \mathbf{a}_c; \mathbf{x}_c)$ (6) evaluated with respect to $\tilde{\mathbf{f}}$ (for a given $\mathbf{a}_c$) and

$$[\mathbf{V}_{c,r}]_{\cdot,k} \triangleq \frac{d^r}{df_k^r}[\mathbf{V}_c]_{\cdot,k}, \tag{19}$$

with $r = 1, 2$ and $k = 1, 2, \ldots, K$, is the rth order column-wise derivative of $\mathbf{V}_c$. In (16), the step size μ is set equal to one unless no increase in the value of $L_{\mathrm{DML}}(\mathbf{f}, \mathbf{a}_c; \mathbf{x}_c)$ is observed; otherwise, it is reduced (usually halved). The Newton-type method expressed by (16)–(18) is repeated until

[2]In our computer simulations, this threshold was selected to minimize the detection of false (i.e., ghost) spectral components (the Chi-Square test has been adopted [33, Par. 4.7.2]).

[3]In (17) and (18) the dependence on $\mathbf{f}$ is omitted for simplicity.

convergence[4] or until the maximum number of iterations is reached. At the end of the last iteration, whose index is denoted $\bar{\alpha}$, the estimate $\hat{\mathbf{f}}$ of $\mathbf{f}$ is set equal to $\mathbf{f}_{\bar{\alpha}+1}$.

Step 5) In this step, **Step 3)** is executed again for the residual periodogram $\mathcal{P}_c(\mathbf{x}_c - \mathbf{P}_c(\hat{\mathbf{f}})\mathbf{x}_c))$ rather than for $\mathcal{P}_c(\mathbf{x}_c)$, and the frequencies corresponding to each local maximum are collected in the vector $\hat{\mathbf{f}}'_0$. If this last vector is empty, the procedure is stopped; otherwise, the process proceeds with **Step 4)**, but the input vector $[\hat{\mathbf{f}}; \hat{\mathbf{f}}'_0]$ is used.

It is important to point out that:

a) The repetition of **Step 3)** in **Step 5)** is usually unnecessary or needs to be performed only once.
b) The residual periodogram $\mathcal{P}_c(\mathbf{x}_c - \mathbf{P}_c(\hat{\mathbf{f}})\mathbf{x}_c))$ needs to be computed only around the active indices. This implies that its complexity is just $\mathcal{O}(K^2)$ rather than $\mathcal{O}(N^2)$.
c) At the end of **Step 5)**, the estimate $\hat{K}$ of the overall number of overlapped complex exponentials (i.e., K) is given by the size of the frequency vector $\hat{\mathbf{f}}$.

III. ADAPTATION OF THE COMPLEX MF SIGNAL MODEL AND PN METHOD TO THE REAL MF PROBLEM

In this section, we adapt the results illustrated in the previous section to the estimation of multiple real frequencies. In this case, $x_c(t)$ (3) is replaced by the real signal

$$x(t) \triangleq \sum_{k=1}^{K} a_k \cos(2\pi \nu_k t + \phi_k) + w(t), \tag{20}$$

where a_k, ν_k and ϕ_k denote the unknown real amplitude, frequency and phase, respectively, of the kth sinusoid (with $k = 1, 2, \ldots, K$), and $w(t)$ is a band-limited real Gaussian noise process having zero mean. Using the angle-sum identity for the cosine, (20) can be rewritten as

$$x(t) = \sum_{k=1}^{K} [\cos(2\pi \nu_k t), \sin(2\pi \nu_k t)] \begin{bmatrix} a_k \cos(\phi_k) \\ -a_k \sin(\phi_k) \end{bmatrix} + w(t). \tag{21}$$

Then, sampling $x(t)$ at the instants $\{(n-1)T; 1 \le n \le N\}$ with sampling period T produces the N-dimensional vector $\mathbf{x}$, such that $[\mathbf{x}]_n \triangleq x((n-1)T)$. Based on (21), it can be shown that

$$\mathbf{x} = \mathbf{V}(\mathbf{f}^{(d)})\mathbf{a} + \mathbf{w}, \tag{22}$$

where

- $[\mathbf{f}]_k \triangleq \nu_k T$, $k = 1, 2, \ldots, K$, and $\mathbf{f}^{(d)}$ follows the notation in (1);
- for any $2K$-dimensional vector $\boldsymbol{\gamma}$, $\mathbf{V}(\boldsymbol{\gamma})$ is an $N \times (2K)$ *signature matrix* such that

$$[\mathbf{V}(\boldsymbol{\gamma})]_{n,2k-1} \triangleq \cos(2\pi[\boldsymbol{\gamma}]_{2k-1}(n-1)),$$
$$[\mathbf{V}(\boldsymbol{\gamma})]_{n,2k} \triangleq \sin(2\pi[\boldsymbol{\gamma}]_{2k}(n-1)), \tag{23}$$

and

$$[\mathbf{a}]_{2k-1} \triangleq a_k \cos(\phi_k), \qquad [\mathbf{a}]_{2k} \triangleq -a_k \sin(\phi_k),$$
$$[\mathbf{w}]_n \triangleq w((n-1)T).$$

with $1 \le n \le N$ and $1 \le k \le K$.

Note that the model (22) is mathematically equivalent to (4) except for the following:

1) Equation (22) is a real model whereas (4) is a complex one.
2) In (22), the columns of $\mathbf{V}(\mathbf{f}^{(d)})$ depend on the components of $\mathbf{f}$ in a pairwise fashion since both $[\mathbf{V}(\mathbf{f}^{(d)})]_{\cdot,2k-1}$ and $[\mathbf{V}(\mathbf{f}^{(d)})]_{\cdot,2k}$ depend on the same frequency f_k (with $k = 1, 2, \ldots, K$). In (4), instead, each column of $\mathbf{V}_c(\mathbf{f})$ depends on a single frequency, that is $[\mathbf{V}_c(\mathbf{f})]_k$ depends exclusively on f_k (with $k = 1, 2, \ldots, K$).

Taking into account the similarities between (22) and (4) as well as the last two differences, we can adapt the results illustrated in the previous section for the complex MF problem to the real counterpart. If the elements of $\mathbf{w}$ are i.i.d., evaluating the DML estimate $\hat{\mathbf{f}}$ of $\mathbf{f}$ in (22) requires maximizing the cost function

$$\bar{L}_{\mathrm{DML}}(\tilde{\mathbf{f}}, \tilde{\mathbf{a}}; \mathbf{x}) \triangleq -\|\mathbf{x} - \mathbf{V}(\tilde{\mathbf{f}}^{(d)})\tilde{\mathbf{a}}\|^2 \tag{24}$$

with respect to $\tilde{\mathbf{f}}$ and $\tilde{\mathbf{a}}$. Following the same approach described in the complex MF case (see (7)–(10)) for $\bar{L}_{\mathrm{DML}}(\tilde{\mathbf{f}}, \tilde{\mathbf{a}}; \mathbf{x})$ (24), leads to the concentrated cost function

$$\bar{L}(\tilde{\mathbf{f}}; \mathbf{x}) \triangleq \mathbf{x}^T \mathbf{P}(\tilde{\mathbf{f}}^{(d)})\mathbf{x}, \tag{25}$$

where $\mathbf{P}(\tilde{\mathbf{f}}^{(d)}) \triangleq \mathbf{V}(\tilde{\mathbf{f}}^{(d)})\mathbf{V}(\tilde{\mathbf{f}}^{(d)})^{\dagger}$. Then, steps **1)** to **5)** can also be followed for the computation of the real DML estimates. However, the following differences must be taken into account:

1) The "c" subscript appearing in various variables must be removed.
2) The vector $\mathbf{f}$ is replaced by $\mathbf{f}^{(d)}$.
3) In **Step 1)** the vector $\mathcal{P}_c(\mathbf{x}_c)$ (see (12)) is replaced by $\mathcal{P}(\mathbf{x})$, that represents a "real" periodogram whose $(p+1)$ element is (see (25))

$$[\mathcal{P}(\mathbf{x})]_{p+1} \triangleq \frac{1}{2}\bar{L}\left(\frac{p}{bN}; \mathbf{x}\right)$$
$$= \frac{1}{2}\mathbf{x}^T \mathbf{P}\left(\left[\frac{p}{bN}; \frac{p}{bN}\right]\right)\mathbf{x} \tag{26}$$

for $p = 1, 2, \ldots, bN/2 - 1$, where bN is assumed to be even. The periodogram $\mathcal{P}(\mathbf{x})$ can be obtained[5] from the half-length DFT of $\mathbf{x}$, given by the $(bN/2)$-length vector

$$[\mathbf{x}_F]_{p+1} \triangleq \sum_{n=0}^{N-1} [\mathbf{x}]_n e^{-j2\pi pn/(bN)}. \tag{27}$$

Note that:

- Only half of the DFT is computed in this case, since the size of $\mathbf{x}_F$ is $bN/2$ rather than bN.

[4] In practice, the Newton-type refinement is stopped if no relevant increase in the value of the cost function $L_c(\mathbf{f}; \mathbf{x}_c)$ (10) is observed.

[5] See App for further details on this step.

- Computationally, both $\mathcal{P}_c(\mathbf{x})$ and $\mathcal{P}(\mathbf{x})$ have $\mathcal{O}(N \log N)$ order, but $\mathcal{P}_c(\mathbf{x})$ is somewhat less complex, given that $\mathcal{P}(\mathbf{x})$ involves the evaluation of the formula derived in App.
- $\mathcal{P}_c(\mathbf{x}) \approx \mathcal{P}(\mathbf{x})$ for frequencies not in the vicinity of $f = 0$. Thus, $\mathcal{P}(\mathbf{x})$ can be replaced by $\mathcal{P}_c(\mathbf{x})$ in our method for solving the real MF problem if there is no significant spectral content around $f = 0$.

4) **Step 4)** is modified by

- Replacing the Hermitian operator $(\cdot)^H$ with the transpose operator $(\cdot)^T$ in all expressions as the involved matrices are real.
- Applying the *chain rule* for the derivative in the evaluation of the expression of the gradient and the Hessian (see (17) and (18), respectively), because the columns of $\mathbf{V}(\mathbf{f}^{(d)})$ depend on each element of $\mathbf{f}$ in a pair-wise fashion rather than individually (for this reason, (17) and (18) cannot be used in this case). Since $\mathbf{f}^{(d)}$ is a function of $\mathbf{f}$ whose Jacobian is the $2K \times K$ matrix $\mathbf{J}$, with

$$[\mathbf{J}]_{r,k} \triangleq \begin{cases} 1 & \text{if } r = 2k \text{ or } r = 2k-1, \\ 0 & \text{otherwise,} \end{cases} \tag{28}$$

for $k = 1, 2, \ldots, K$, it is only required to left-multiply the gradient by $\mathbf{J}^T$ and left- and right-multiply the Hessian by $\mathbf{J}^T$ and $\mathbf{J}$. The resulting expressions for the gradient and the Hessian are

$$\mathbf{g}(\tilde{\mathbf{f}}^{(d)}, \mathbf{a}) \triangleq 2\,\mathbf{J}^T\big(\mathbf{a} \odot (\mathbf{V}_1^T(\mathbf{x} - \mathbf{V}\mathbf{a}))\big), \tag{29}$$

and

$$\mathbf{H}(\tilde{\mathbf{f}}^{(d)}, \mathbf{a}) \triangleq -2\,\mathbf{J}^T\Big((\mathbf{a}\mathbf{a}^T) \odot (\mathbf{V}_1^T\mathbf{V}_1) - \operatorname{diag}\big(\mathbf{a} \odot (\mathbf{V}_2^T(\mathbf{x} - \mathbf{V}\mathbf{a}))\big)\Big)\mathbf{J}, \tag{30}$$

respectively. Note that: a) in the *right hand side* (RHS) of the last equations, the dependence on $\tilde{\mathbf{f}}^{(d)}$ has been omitted for simplicity; b) the effect of multiplying by $\mathbf{J}$ (or $\mathbf{J}^T$) is simply to combine pairs of adjacent columns (or rows) of the matrix it right- (or left-) multiplies.

IV. COMPUTATIONALLY EFFICIENT IMPLEMENTATION OF THE DML ESTIMATOR FOR THE REAL MF PROBLEM

The DML estimator described in the previous section may appear computationally daunting, given that it involves matrix functions such as the gradient and Hessian in (29) and (30) or the projection matrix $\mathbf{P}(\tilde{\mathbf{f}}^{(d)})$ in (25). However, a closer analysis reveals two relevant features.[6] First, the computed functions *exclusively* depend on the autocorrelation of the signature matrix $\mathbf{V}(\tilde{\mathbf{f}}^{(d)})$, or on its correlation with the data vector $\mathbf{x}$. Second, these correlations are the only computations whose complexity is proportional to the snapshot length N, except for the inner product $\mathbf{x}^T\mathbf{x}$ which, being constant, needs to be computed only once. From these considerations, it can be inferred that the overall complexity of the DML estimator can be made independent of N and small if an efficient computation method for the abovementioned correlations is found. In the sequel, we provide additional details and present an efficient method for computing correlations with complexity independent of N. To begin, we note that all computations in the proposed estimator depend on the correlations[7]

$$\mathcal{R}(\mathbf{V}, \mathbf{V}),\ \mathcal{R}(\mathbf{V}, \mathbf{V}_1),\ \mathcal{R}(\mathbf{V}, \mathbf{V}_2),\ \mathcal{R}(\mathbf{V}_1, \mathbf{V}_1) \tag{31}$$

$$\mathcal{R}(\mathbf{V}, \mathbf{x}),\ \mathcal{R}(\mathbf{V}_1, \mathbf{x}),\ \mathcal{R}(\mathbf{V}_2, \mathbf{x}). \tag{32}$$

To show a few examples, the cost function in (25) can be written as

$$\mathbf{x}^T\mathbf{P}(\tilde{\mathbf{f}}^{(d)})\mathbf{x} = \mathcal{R}(\mathbf{V}, \mathbf{x})^T\mathcal{R}(\mathbf{V}, \mathbf{V})^{-1}\mathcal{R}(\mathbf{V}, \mathbf{x}). \tag{33}$$

and the gradient and Hessian in (29) as

$$\mathbf{g}(\tilde{\mathbf{f}}^{(d)}, \mathbf{a}) = 2\,\mathbf{J}^T\big(\mathbf{a} \odot (\mathcal{R}(\mathbf{V}_1, \mathbf{x}) - \mathcal{R}(\mathbf{V}, \mathbf{V}_1)^T\mathbf{a})\big), \tag{34}$$

and

$$\mathbf{H}(\tilde{\mathbf{f}}^{(d)}, \mathbf{a}) = -2\,\mathbf{J}^T\Big((\mathbf{a}\mathbf{a}^T) \odot \mathcal{R}(\mathbf{V}_1, \mathbf{V}_1) - \operatorname{diag}\big(\mathbf{a} \odot (\mathcal{R}(\mathbf{V}_2, \mathbf{x}) - \mathcal{R}(\mathbf{V}, \mathbf{V}_2)^T\mathbf{a})\big)\Big)\mathbf{J}, \tag{35}$$

respectively. Note that if all correlations (31)–(32) are available then Step 4) can be computed in $\mathcal{O}(K^3)$ operations, i.e, with a complexity that is independent of N. Besides, the only $\mathcal{O}(K^3)$ operations in this step are those required to solve the two linear systems

$$\mathcal{R}(\mathbf{V}, \mathbf{V})\hat{\mathbf{a}}_\alpha = \mathcal{R}(\mathbf{V}, \mathbf{x}), \tag{36}$$

$$\mathbf{H}(\tilde{\mathbf{f}}^{(d)}, \hat{\mathbf{a}}_\alpha)\mathbf{y} = \mathbf{g}(\tilde{\mathbf{f}}^{(d)}, \hat{\mathbf{a}}_\alpha), \tag{37}$$

where $\mathbf{y}$ is a $K \times 1$ real vector. Actually, since these linear systems are real and symmetric, each of them can be solved in $K^3/3 + 2K^2$ flops using the Cholesky decomposition (see Algs. 4.2.1 and 3.1.1 in [34]).

Let us now address the problem of computing the correlations (31)–(32) with $\mathcal{O}(1)$ in N. The correlations in (31) are independent of $\mathbf{x}$ and consist of trigonometric sums for which closed-form formulas exist. Such formulas are based on the product-to-sum identity of two cosines and geometric series. More precisely, they can be expressed in terms of the function

$$C(x, y; \alpha, \beta) \triangleq \sum_{n=0}^{N-1} \cos(2\pi n x + \alpha)\cos(2\pi n y + \beta) = \frac{1}{2}\operatorname{Re}\{e^{j(\alpha-\beta)}S(x-y) + e^{j(\alpha+\beta)}S(x+y)\} \tag{38}$$

[6] These features were first noticed and exploited in [27], and play an important role in the minimization of the usual cost functions defined in ML frequency estimation and in DOA estimation.

[7] Here and in the sequel, we omit the dependence of the signature matrix on $\tilde{\mathbf{f}}^{(d)}$ to ease reading.

and its derivatives, if a proper combination of the values 0 and $-\pi/2$ is assigned to α and β; here, $S(z) \triangleq (e^{j2\pi Nz} - 1)/(e^{j2\pi z} - 1)$ represents the closed-form expression of the geometric sum $1 + e^{j2\pi z} + \ldots + e^{j2\pi(N-1)z}$. Note that, since the expression of $C(x, y; \alpha, \beta)$ in (38) can be differentiated in closed form in x and y to any order, the computational cost of all the ($\mathbf{x}$-free) correlations listed in (31) is $\mathcal{O}(K^2)$ (i.e., it is $\mathcal{O}(1)$ in N).

The $\mathbf{x}$-dependent correlations listed in (32) can be accurately interpolated with $\mathcal{O}(1)$ complexity from a few elements of $\mathbf{x}_F$ (see (27)). Therefore, we do not need to directly compute the correlation

$$\mathcal{R}(\mathbf{V}_q, \mathbf{x}) \triangleq \mathbf{V}_q(\tilde{\mathbf{f}}^{(d)})^T\mathbf{x}. \tag{39}$$

according to its definition (the computational cost of this task would be $\mathcal{O}(N)$). To demonstrate this, we note that

$$[\mathcal{R}(\mathbf{V}_q, \mathbf{x})]_{2k-1:2k} = \begin{bmatrix} \mathrm{Re}\{G_q(\tilde{f}_k; \mathbf{x})\} \\ -\mathrm{Im}\{G_q(\tilde{f}_k; \mathbf{x})\} \end{bmatrix}, \tag{40}$$

for $1 \leq k \leq K$, where

$$G_q(f; \mathbf{x}) \triangleq \frac{d^q}{df^q} \sum_{n=0}^{N-1} [\mathbf{x}]_{n+1} e^{-j2\pi nfT} \tag{41}$$

represents the qth derivative of the DTFT of $\mathbf{x}$ (with $q \geq 0$). Thus, the problem of efficiently evaluating $\mathcal{R}(\mathbf{V}_q, \mathbf{x})$ is equivalent to that of efficiently computing the DTFT $G_0(\tilde{f}; \mathbf{x})$ and its derivatives. Since $G_0(f; \mathbf{x})$ is a band-limited signal in the $\tilde{f}$ variable and its samples are known with oversampling factor[8] b, an interpolation formula of the form

$$G_q(f; \mathbf{x}) \approx \sum_{\alpha=-P}^{P} c_{q,\alpha}(u(f)) G_0\Big(\frac{n(f) - p}{bN}; \mathbf{x}\Big) \tag{42}$$

can be used for its evaluation for any $q \geq 0$; here, P is the truncation index, $c_{q,\alpha}(u(f))$ is the qth coefficient of the interpolator and

$$n(f) \triangleq \lfloor 1/2 + bNf \rfloor, \; u(f) \triangleq f - n(f)/(bN), \tag{43}$$

so that $f = n(f)/(bN) + u(f)$ represents a mod-$(1/(bN))$ decomposition of f (further details regarding the available interpolation formulas and their coefficients can be found in [35]). It is important to point out that

1) The $2P + 1$ samples $\{G_0((n(f) - p)/(bN); \mathbf{x}); \; p = -P, -P + 1, \ldots, P\}$ appearing in the RHS of (42) are known because they are elements of $\mathbf{x}_F$ (with a proper index mapping).
2) According to [35], the interpolation error due to the use of (42) decreases exponentially with P. In practice, if $b = 2$, selecting P between 3 and 6 is sufficient.
3) The evaluation of (42), including the coefficients $c_{q,\alpha}(u)$, requires a small number of flops if the so-called *barycentric interpolator* is employed [35].
4) The computation of the x-dependent correlations listed in (32) require $\mathcal{O}(1)$ operations for each frequency $\bar{f}_k$; therefore, the overall computational cost is $\mathcal{O}(K)$.

The computationally efficient implementation of the proposed estimator, called the PN algorithm, as in the complex case, is summarized in Algorithm 1.

[8]Note that these samples are the elements of $\mathbf{x}_F$ (see (27)).

V. NUMERICAL RESULTS

In this section, we compare, in terms of accuracy and computational complexity, the PN algorithm with the methods proposed by Djukanović [36], Ye et al. [7], [37], and Candan and Çelebi [38] (denoted Alg-D, Alg-Y, and Alg-C, respectively, in the following). Moreover, we assess the improvement in the estimation accuracy provided by the *expectation maximization* (EM) algorithm [17] when initialized by each of the above-mentioned algorithms. Although Alg-D, Alg-Y and Alg-C are single frequency estimators, they can also be used for the estimation of multiple sinusoids through a serial cancellation procedure consisting of the estimation of the dominant sinusoid followed by its subtraction from the available signal samples [39]. Two different scenarios were considered in our computer simulations. In all of them, $N = 1024$ has been selected for the number of samples, and, for any k, the phases of the K sinusoids have been randomly selected over the interval $[0, 2\pi]$, each independently of the other ones.

The specific features of the simulated scenarios can be summarized as follows:

Scenario #1 (**S1**): This is characterized by $K = 4$, that is, by four tones, whose amplitudes are $a_1 = 1$, $a_2 = 0.782$, $a_3 = 0.873$ and $a_4 = 0.687$. The frequency f_i of the ith sinusoid is given by $f_i = f_0 + \Delta f_i$ (with $i = 1, 2, 3$ and 4), where f_0 is uniformly distributed over the interval $[10/N, 30/N]$, $\Delta f_1 = 0$, $\Delta f_2 = 1.5/N$, $\Delta f_3 = 1.5/N$ and $\Delta f_4 = 10.5/N$.

Scenario #2 (**S2**): This is characterized by $K = 4$, that is, by four tones, with an amplitude equal to one. Moreover, the frequency f_0 of the first tone is uniformly distributed over the interval $[10/N, 20/N]$, whereas that of the kth ($k = 1, 2, 3$) tone is $f_k = f_0 + d\,k/N$. Here, d (with $d = 1, 2, 3$) is assumed to be a non-negative parameter controlling the frequency spacing between adjacent tones.

The *signal-to-noise ratio* (SNR) range $[-10, 20]$ dB and the following parameters were selected: a) oversampling factor $b = 2$, interpolation order $P = 6$ and maximum number of iterations $N_{\mathrm{it}} = 5$ for the PN algorithm, b) number of frequency bins employed in filtering equal to 1 for Alg-D (this corresponds to selecting $K = 0$ in that algorithm (see [36, Subsec. III.A]), c) overall number of iterations $Q = 3$ for Alg-Y, d) oversampling factor and overall number of iterations equal to 2 and 6, respectively, for Alg-C, e) number of grid nodes equal to 11 and overall number of iterations equal to 3 for the EM algorithm, and f) false-alarm probability equal to 10^{-5} in the

Algorithm 1 Periodogram-Newton Algorithm

Input: vector $\mathbf{x}$ (22), detection threshold ϵ, oversampling factor b, interpolation order P, and maximum number of iterations N_{it}.

1 **Initialization:**

a) Compute the periodogram $\mathcal{P}(\mathbf{x})$ from the DFT of $\mathbf{x}$ (see (26) and (27)) ($\mathcal{O}(N \log N)$ complexity).

b) Store the indices of the elements of $\mathcal{P}(\mathbf{x})$ with amplitude exceeding ϵ in the set $\mathcal{I}$ ($\mathcal{O}(N)$ complexity).

c) Find out the indices p in $\mathcal{I}$ such that $[\mathcal{P}(\mathbf{x})]_p$ is a local maximum of the vector $\mathcal{P}(\mathbf{x})$ and store their corresponding frequencies $(p-1)/(bN)$ in the vector $\hat{\mathbf{f}}_0$ ($\mathcal{O}(K)$ complexity).

2 **Frequency and amplitude refinement:**

for $\alpha = 0$ **to** N_{it} **do**

d) Compute the refined estimate $\hat{\mathbf{a}}_\alpha$ (see (15)) of the amplitudes according to the methods described in Sec. IV, that is as $\mathcal{R}(\mathbf{V},\mathbf{V})^{-1}\mathcal{R}(\mathbf{V},\mathbf{x})$ ($\mathcal{O}(K^3)$ complexity).

e) Compute the refined estimate of the frequencies as $\hat{\mathbf{f}}_{\alpha+1} = \hat{\mathbf{f}}_\alpha - \mu\mathbf{H}^{-1}(\hat{\mathbf{f}}_\alpha^{(d)}, \hat{\mathbf{a}}_\alpha)\mathbf{g}(\hat{\mathbf{f}}_\alpha^{(d)}, \hat{\mathbf{a}}_\alpha)$; here, $\mathbf{g}$ (29) and $\mathbf{H}$ (30) are computed according to the method described in Sec. IV, that is as $2\boldsymbol{J}^T(\hat{\mathbf{a}}_\alpha \odot (\mathcal{R}(\mathbf{V}_1,\mathbf{x}) - \mathcal{R}(\mathbf{V}_1,\mathbf{V})\hat{\mathbf{a}}_\alpha))$ and $-2\,\mathbf{J}^T((\hat{\mathbf{a}}_\alpha\hat{\mathbf{a}}_\alpha^T) \odot \mathcal{R}(\mathbf{V}_1,\mathbf{V}_1) - \text{diag}(\hat{\mathbf{a}}_\alpha \odot (\mathcal{R}(\mathbf{V}_2,\mathbf{x}) - \mathcal{R}(\mathbf{V}_2,\mathbf{V})\hat{\mathbf{a}}_\alpha)))\mathbf{J}$, respectively ($\mathcal{O}(K^3)$ complexity).

f) The Newton-type refinement of steps **d)** and **e)** is stopped if no relevant increase in the value of the cost function $\bar{L}(\tilde{\mathbf{f}};\mathbf{x})$ (25) is observed.

end

Set $\hat{\mathbf{f}}$ equal to $\hat{\mathbf{f}}_{\tilde{\alpha}+1}$.

3 **Residual periodogram computation:**

g) For each index p in $\mathcal{I}$, compute the residual periodogram sample as

$$\|\mathcal{R}(\bar{\mathbf{V}},\mathbf{x}) - \mathcal{R}(\bar{\mathbf{V}},\mathbf{V})\mathbf{b}\|^2; \tag{44}$$

here, $\mathbf{b} \triangleq \hat{\mathbf{a}}_{\tilde{\alpha}}$ (see **d)**) and

$$\bar{\mathbf{V}} = \mathbf{V}([p/(bN); p/(bN)]).$$

Since the computational cost of (44) is $\mathcal{O}(K)$ and cardinality of $\mathcal{I}$ is K, the overall cost of this step is $\mathcal{O}(K^2)$.

h) If any peak with amplitude greater than ϵ appears in the residual periodogram, include it as a new element of the vector $\hat{\mathbf{f}}$ and go to step **d)**; otherwise, go to **Output**.

4 **Output:** 1) The estimates $\hat{\mathbf{f}}$ and $\hat{\mathbf{a}}$ of $\mathbf{f}$ and $\mathbf{a}$; 2) the estimate $\hat{K}$ of K as the cardinality of $\hat{\mathbf{f}}$.

computation of the noise threshold ϵ employed in frequency detection.

Our computer simulations have allowed us to assess: 1) the *root mean square error* (RMSE_f) achieved in the frequency estimation of the first (i.e., of the strongest) tone[9]; 2) the computational complexity in Megaflops[10]; and 3) the average number of detected sinusoids. The aforementioned performance metrics have been computed by running 10^4 Montecarlo simulations.

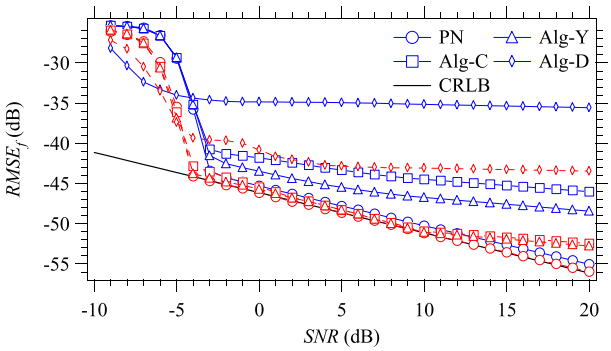

FIGURE 1. Root mean square error and CRLB versus SNR (first scenario). Dashed red (solid blue) lines refer to the accuracy achieved when the EM is (not) used. The PN, Alg-C, Alg-Y and Alg-D are considered. The CRLB is also shown for comparison.

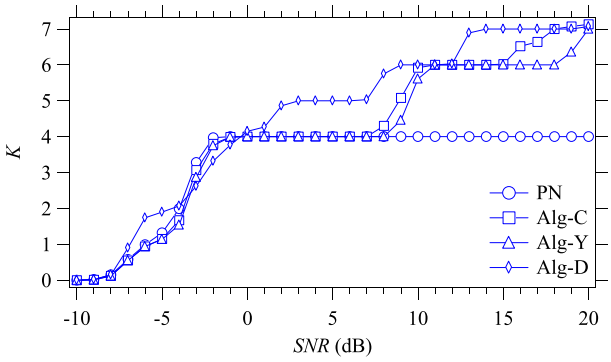

FIGURE 2. Average number of detected sinusoids versus SNR (first scenario). The PN, Alg-C, Alg-Y and Alg-D are considered.

Some numerical results for **S1** are shown in Figs. 1, 2, and 3. From these results it can be inferred that: a) the PN algorithm accuracy is very close to the *Cramér Rao lower bound* (CRLB) in the SNR range $[-4, 20]$ dB; b) the RMSE_f reduction achieved through the use of the EM algorithm is significant for Alg-D, Alg-Y, and Alg-C; c) the RMSE_f of Alg-D is far from the CRLB for any value of SNR even if the EM is employed; d) Alg-C and Alg-D (with EM refinement) depart from the CRLB for an SNR greater than 10 dB; e) the average number of detected sinusoids for the PN algorithm is equal to 4 if the SNR is greater than -2 dB, whereas it is greater than 4 for the Alg-D, Alg-C, and Alg-Y

[9]This choice is motivated by the fact that, as K is unknown, the overall number of tones detected by each of the considered algorithms is not necessarily correct.

[10]The computational complexity of each algorithm has been accurately evaluated by counting the number of flops executed in all its steps.

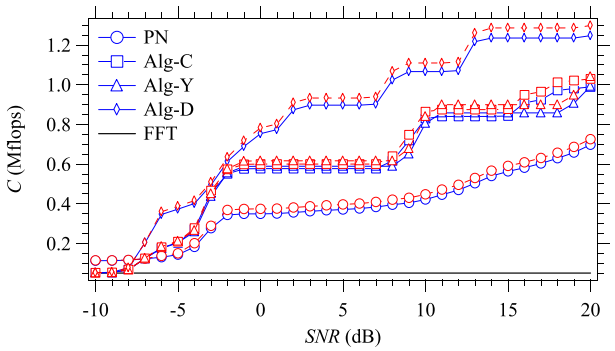

FIGURE 3. Computational cost versus SNR (first scenario). Dashed red (solid blue) lines refer to the case in which frequency estimates are (not) refined by the EM algorithm. The PN, Alg-C, Alg-Y and Alg-D are considered. The computational cost of FFT processing is also shown for comparison.

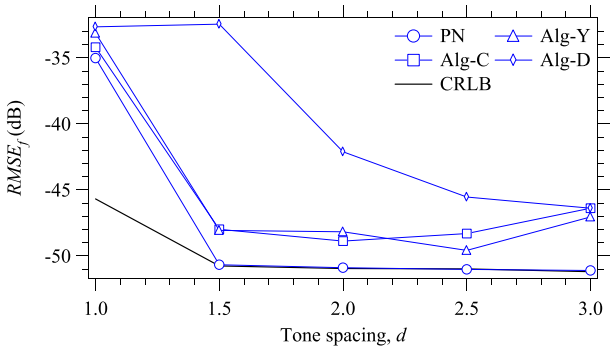

FIGURE 4. Root mean square error and CRLB versus tone spacing (second scenario). The PN, Alg-C, Alg-Y and Alg-D are considered. The CRLB is also shown for comparison.

if the SNR exceeds 0 dB, 8 dB and 9 dB, respectively[11]; f) the PN algorithm is more computationally efficient than Alg-C, Alg-Y, and Alg-D for any SNR greater than the SNR threshold (i.e., -2 dB); g) the computational cost added by the EM refinement step is small with respect to the overall computational cost of the algorithms themselves in the considered scenario.

Some of the numerical results for **S2** are presented in Fig. 4. Our results show that: 1) all the considered algorithms depart from the CRLB for $d = 1$; 2) the PN algorithm attains the CRLB for $d \geq 1.5$; 3) the RMSE$_f$ of Alg-C and Alg-Y is approximately 3 dB far from the CRLB for $1.5 \leq d \leq 2.5$; 4) the RMSE$_f$ of Alg-C, Alg-Y and Alg-D departs from the CRLB for $d = 3$. The last result is due to the fact that, for $d = 3$, the average number of estimated tones differs from its true value (i.e., from 4). This entails an increase in the RMSE$_f$ observed for the first tone.

These results lead to the conclusion that, in the presence of multiple sinusoids, the PN algorithm achieves the best performance-complexity trade-off.

[11] Note that as the SNR increases, the detection threshold ϵ decreases; this implies that the error accumulation affecting the serial cancellation procedure employed for the sequential detection of multiple tones can potentially lead to the detection of false (i.e., ghost) spectral components.

VI. CONCLUSION

A novel estimator for multiple real tones has been developed. It employs the periodogram to obtain initial coarse estimates of multiple frequencies, and a combination of AP and a Newton-type method to refine them. The main strength of the proposed estimator is its low complexity. In fact, once a single FFT (requiring $\mathcal{O}(N \log N)$ operations) is computed, the refinement of the frequency estimates is independent of the snapshot size and requires at most $\mathcal{O}(K^3)$ operations. Our numerical results show that the proposed method achieves a better performance-complexity trade-off than other estimators available in the technical literature.

APPENDIX
COMPUTATION OF REAL PERIODOGRAM FROM DISCRETE-TIME FOURIER TRANSFORM (DTFT)

In this Appendix, a method for the efficient computation of the periodogram $\mathcal{P}(\mathbf{x})$ (26) from $\mathbf{x}_F$ (27) is derived. First of all, let $c(f;\mathbf{x})$ denote the Discrete-Time Fourier Transform (DTFT) of $\mathbf{x}$, i.e.,

$$c(f;\mathbf{x}) \triangleq \sum_{n=0}^{N-1} [\mathbf{x}]_{n+1} e^{-j2\pi nf}. \tag{45}$$

Based on (45), it can be shown that (see (26) and (27))

$$[\mathbf{x}_F]_{p+1} = c(f;\mathbf{x}) \tag{46}$$

and

$$[\mathcal{P}(\mathbf{x})]_{p+1} = \frac{1}{2}\bar{L}(f;\mathbf{x}) \tag{47}$$

for $f = p/(bN)$. If we set $\tilde{\mathbf{f}} = f$ in (25), where f denotes an arbitrary scalar frequency, $\bar{L}(f;\mathbf{x})$ (25) represents the square norm of the orthogonal projection of $\mathbf{x}$ onto the span of $\mathbf{V}(f^{(d)})$ (23). In this case, the matrix $\mathbf{V}(f^{(d)})$ has the following properties: a) its size is $N \times 2$; b) its first and second column are formed by cosines and sines, respectively, all at the same frequency f; c) it has the same column span as the complex matrix $\mathbf{V}_c([f;-f])$, defined in (5). Thus, if we define $\boldsymbol{\gamma} \triangleq [f;-f]$, $L(f;\mathbf{x})$ can be computed by projecting $\mathbf{x}$ onto the span of $\mathbf{V}_c(\boldsymbol{\gamma})$, i.e. as

$$\begin{aligned} L(f;\mathbf{x}) &= \mathbf{x}^T \mathbf{P}_c(\boldsymbol{\gamma})\mathbf{x} \\ &= \mathbf{x}^T \mathbf{V}_c(\boldsymbol{\gamma})(\mathbf{V}_c(\boldsymbol{\gamma})^H \mathbf{V}_c(\boldsymbol{\gamma}))^{-1} \mathbf{V}_c(\boldsymbol{\gamma})^H \mathbf{x}. \end{aligned} \tag{48}$$

Note that: a) the term $\mathbf{V}_c(\boldsymbol{\gamma})^H\mathbf{x}$ appearing in the RHS of (48) can be expressed as (see (45))

$$\mathbf{V}_c(\boldsymbol{\gamma})^H \mathbf{x} = \begin{pmatrix} c(f;\mathbf{x}) \\ c(f;\mathbf{x})^* \end{pmatrix} = \begin{pmatrix} 1 & j \\ 1 & -j \end{pmatrix} \cdot \begin{pmatrix} c_R(f;\mathbf{x}) \\ c_I(f;\mathbf{x}) \end{pmatrix}, \tag{49}$$

if notation 5) is adopted; b) the product $\mathbf{V}_c(\boldsymbol{\gamma})^H\mathbf{V}_c(\boldsymbol{\gamma})$ can be expressed as

$$\mathbf{V}_c(\boldsymbol{\gamma})^H \mathbf{V}_c(\boldsymbol{\gamma}) = \begin{pmatrix} N & h(f) \\ h(f)^* & N \end{pmatrix}, \tag{50}$$

where

$$h(f) \triangleq \sum_{n=0}^{N-1} e^{-j4\pi nf} = Ne^{-j2\pi(N-1)f} \frac{\operatorname{sinc}(2Nf)}{\operatorname{sinc}(2f)}. \quad (51)$$

From (50) it is easily inferred that

$$(\mathbf{V}_c(\boldsymbol{\gamma})^H \mathbf{V}_c(\boldsymbol{\gamma}))^{-1} = \frac{1}{N^2 - |h(f)|^2} \begin{pmatrix} N & -h(f) \\ -h(f)^* & N \end{pmatrix}. \quad (52)$$

Finally, substituting (49), (51) and (52) into (48) and expanding the matrix products yields

$$L(f;\mathbf{x}) = \frac{2}{N^2 - h_R(f)^2 - h_I(f)^2} \cdot \left(c_R(f;\mathbf{x}),\ c_I(f;\mathbf{x})\right) \cdot \begin{pmatrix} -h_R(f)+N & -h_I(f) \\ -h_I(f) & h_R(f)+N \end{pmatrix} \cdot \begin{pmatrix} c_R(f;\mathbf{x}) \\ c_I(f;\mathbf{x}) \end{pmatrix}. \quad (53)$$

The last formula allows us to compute $\bar{L}(f;\mathbf{x})$ from the DTFT $c(f;\mathbf{x})$ and, consequently, to obtain $\mathcal{P}(\mathbf{x})$ from $\mathbf{x}_F$; in doing so, we set $f = p/(bN)$, with $p = 0, 1, \ldots, bN/2-1$. □

REFERENCES

[1] S. M. Patole, M. Torlak, D. Wang, and M. Ali, "Automotive radars: A review of signal processing techniques," *IEEE Signal Process. Mag.*, vol. 34, no. 2, pp. 22–35, Mar. 2017.
[2] P. Di Viesti, A. Davoli, G. Guerzoni, and G. M. Vitetta, "Novel deterministic detection and estimation algorithms for colocated multiple-input multiple-output radars," *IEEE Access*, vol. 10, pp. 2216–2255, 2022.
[3] P. D. Viesti, A. Davoli, G. Guerzoni, and G. M. Vitetta, "Recursive algorithms for the estimation of multiple superimposed undamped tones and their application to radar systems," *IEEE Trans. Aerosp. Electron. Syst.*, vol. 59, no. 2, pp. 1834–1853, Apr. 2023.
[4] T. M. Schmidl and D. C. Cox, "Robust frequency and timing synchronization for OFDM," *IEEE Trans. Commun.*, vol. 45, no. 12, pp. 1613–1621, Dec. 1997.
[5] B. G. Quinn and E. J. Hannan, *The Estimation and Tracking of Frequency*, no. 9. Cambridge, U.K.: Cambridge Univ. Press, 2001.
[6] G. Bai, Y. Cheng, W. Tang, S. Li, and X. Lu, "Accurate frequency estimation of a real sinusoid by three new interpolators," *IEEE Access*, vol. 7, pp. 91696–91702, 2019.
[7] S. Ye, J. Sun, and E. Aboutanios, "On the estimation of the parameters of a real sinusoid in noise," *IEEE Signal Process. Lett.*, vol. 24, no. 5, pp. 638–642, May 2017.
[8] Z.-L. Mou, Y.-Q. Tu, P. Chen, and K. Wang, "Accurate frequency estimation of multiple complex and real sinusoids based on iterative interpolation," *Digit. Signal Process.*, vol. 117, Oct. 2021, Art. no. 103173.
[9] J. Luo, Z. Xie, and M. Xie, "Frequency estimation of the weighted real tones or resolved multiple tones by iterative interpolation DFT algorithm," *Digit. Signal Process.*, vol. 41, pp. 118–129, Jun. 2015.
[10] A. Serbes, "Fast and efficient estimation of frequencies," *IEEE Trans. Commun.*, vol. 69, no. 6, pp. 4054–4066, Jun. 2021.
[11] A. M. Walker, "On the estimation of a harmonic component in a time series with stationary independent residuals," *Biometrika*, vol. 58, no. 1, p. 21, Apr. 1971.
[12] D. Rife and R. Boorstyn, "Single tone parameter estimation from discrete-time observations," *IEEE Trans. Inf. Theory*, vol. IT-20, no. 5, pp. 591–598, Sep. 1974.
[13] D. C. Rife and R. R. Boorstyn, "Multiple tone parameter estimation from discrete-time observations," *Bell Syst. Tech. J.*, vol. 55, no. 9, pp. 1389–1410, Nov. 1976.
[14] M. Xu, J. Zhu, J. Fang, N. Zhang, and Z. Xu, "CFAR based NOMP for line spectral estimation and detection," *IEEE Trans. Aerosp. Electron. Syst.*, vol. 59, no. 5, pp. 6971–6990, Nov. 2023.
[15] Y. Bresler and A. Macovski, "Exact maximum likelihood parameter estimation of superimposed exponential signals in noise," *IEEE Trans. Acoust., Speech, Signal Process.*, vol. ASSP-34, no. 5, pp. 1081–1089, Oct. 1986.
[16] I. Ziskind and M. Wax, "Maximum likelihood localization of multiple sources by alternating projection," *IEEE Trans. Acoust., Speech, Signal Process.*, vol. 36, no. 10, pp. 1553–1560, Oct. 1988.
[17] M. Feder and E. Weinstein, "Parameter estimation of superimposed signals using the EM algorithm," *IEEE Trans. Acoust., Speech, Signal Process.*, vol. 36, no. 4, pp. 477–489, Apr. 1988.
[18] J. Zhu, Q. Zhang, P. Gerstoft, M.-A. Badiu, and Z. Xu, "Gridless variational Bayesian line spectral estimation with multiple measurement vectors," *Signal Process.*, vol. 161, pp. 155–164, Aug. 2019.
[19] Q. Zhang, J. Zhu, N. Zhang, and Z. Xu, "Multidimensional variational line spectra estimation," *IEEE Signal Process. Lett.*, vol. 27, pp. 945–949, 2020.
[20] L. Han, X. Liu, N. Zhang, S. Wu, J. Zhu, and Z. Xu, "Two-dimensional multi-snapshot newtonized orthogonal matching pursuit for DOA estimation," *Digit. Signal Process.*, vol. 121, Mar. 2022, Art. no. 103313.
[21] J. Zhu, L. Han, R. S. Blum, and Z. Xu, "Multi-snapshot newtonized orthogonal matching pursuit for line spectrum estimation with multiple measurement vectors," *Signal Process.*, vol. 165, pp. 175–185, Dec. 2019.
[22] B. G. Quinn and P. J. Thomson, "Estimating the frequency of a periodic function," *Biometrika*, vol. 78, no. 1, p. 65, Mar. 1991.
[23] B. G. Quinn, "Estimating frequency by interpolation using Fourier coefficients," *IEEE Trans. Signal Process.*, vol. 42, no. 5, pp. 1264–1268, May 1994.
[24] P. T. Gough, "A fast spectral estimation algorithm based on the FFT," *IEEE Trans. Signal Process.*, vol. 42, no. 6, pp. 1317–1322, Jun. 1994.
[25] J. Li and P. Stoica, "Efficient mixed-spectrum estimation with applications to target feature extraction," *IEEE Trans. Signal Process.*, vol. 44, no. 2, pp. 281–295, Feb. 1996.
[26] E. Aboutanios and B. Mulgrew, "Iterative frequency estimation by interpolation on Fourier coefficients," *IEEE Trans. Signal Process.*, vol. 53, no. 4, pp. 1237–1242, Apr. 2005.
[27] J. Selva, "An efficient Newton-type method for the computation of ML estimators in a uniform linear array," *IEEE Trans. Signal Process.*, vol. 53, no. 6, pp. 2036–2045, Jun. 2005.
[28] J. Selva, "Efficient maximum likelihood estimation of a 2-D complex sinusoidal based on barycentric interpolation," in *Proc. IEEE Int. Conf. Acoust., Speech Signal Process. (ICASSP)*, May 2011, pp. 4212–4215.
[29] J. Selva, "ML estimation and detection of multiple frequencies through periodogram estimate refinement," *IEEE Signal Process. Lett.*, vol. 24, no. 3, pp. 249–253, Mar. 2017.
[30] S. Ye and E. Aboutanios, "An algorithm for the parameter estimation of multiple superimposed exponentials in noise," in *Proc. IEEE Int. Conf. Acoust., Speech Signal Process. (ICASSP)*, Apr. 2015, pp. 3457–3461.
[31] S. Djukanovic and V. Popovic-Bugarin, "Efficient and accurate detection and frequency estimation of multiple sinusoids," *IEEE Access*, vol. 7, pp. 1118–1125, 2019.
[32] A. Serbes and K. Qaraqe, "A fast method for estimating frequencies of multiple sinusoidals," *IEEE Signal Process. Lett.*, vol. 27, pp. 386–390, 2020.
[33] B. Ottersten, M. Viberg, P. Stoica, and A. Nehorai, *Exact and Large Sample Maximum Likelihood Techniques for Parameter Estimation and Detection in Array Processing*. Berlin, Germany: Springer, 1993, pp. 99–151.
[34] G. H. Golub and C. F. Van Loan, *Matrix Computations*. Baltimore, MD, USA: JHU Press, 2013.
[35] J. Selva, "Design of barycentric interpolators for uniform and nonuniform sampling grids," *IEEE Trans. Signal Process.*, vol. 58, no. 3, pp. 1618–1627, Mar. 2010.
[36] S. Djukanovic, "An accurate method for frequency estimation of a real sinusoid," *IEEE Signal Process. Lett.*, vol. 23, no. 7, pp. 915–918, Jul. 2016.
[37] S. Ye, J. Sun, and E. Aboutanios, "Corrections to 'on the estimation of the parameters of a real sinusoid in noise'[May 17 638-642]," *IEEE Signal Process. Lett.*, vol. 25, no. 7, p. 1115, Jul. 2018.

[38] Ç. Candan and U. Çelebi, "Frequency estimation of a single real-valued sinusoid: An invariant function approach," *Signal Process.*, vol. 185, Aug. 2021, Art. no. 108098.
[39] M. D. Macleod, "Fast nearly ML estimation of the parameters of real or complex single tones or resolved multiple tones," *IEEE Trans. Signal Process.*, vol. 46, no. 1, pp. 141–148, Jan. 1998.

PASQUALE DI VIESTI (Graduate Student Member, IEEE) received the bachelor's and master's degrees (cum laude) in electronic engineering from the University of Modena and Reggio Emilia, Italy, in 2016 and 2018, respectively, and the Ph.D. degree in automotive for intelligent mobility from the University of Bologna, in October 2021. He is currently a Research Fellow with the University of Modena and Reggio Emilia. His main research interests include statistical signal processing and MIMO radars.

JESUS SELVA received the M.Sc. degree in communications engineering from the Polytechnic University of Valencia (UPV), Valencia, Spain, in 1994, the M.Sc. degree in mathematics from National Distance Education University, Madrid, Spain, in 2000, and the Ph.D. degree in communications engineering from the Polytechnic University of Catalonia, Barcelona, Spain, in 2004. From 1995 to 1996, he was a Grant Holder with UPV. From 1996 to 1998, he was a Trainee with the Spanish Ministry of Education, European Space Agency. From 1998 to 2004, he was a Researcher with the German Aerospace Centre, Oberpfaffenhofen, Germany. From 2004 to 2011, he was a Juan de la Cierva and Ramon y Cajal Research Fellow with the University of Alicante, San Vicente, Spain. Since 2012, he has been an Associate Professor with the University of Alicante. His main research interests include interpolation for signal processing, sampling theory, navigation systems, synchronization circuits, array processing, and estimation theory.

GIORGIO M. VITETTA (Senior Member, IEEE) received the Dr.Ing. (cum laude) and Ph.D. degrees in electronic engineering from the University of Pisa, Italy, in 1990 and 1994, respectively. Since 2001, he has been a Full Professor of telecommunications with the University of Modena and Reggio Emilia. He has co-authored more than 100 papers published in international journals and on the proceedings of international conferences. He has co-authored the book *Wireless Communications: Algorithmic Techniques* (John Wiley, 2013). His main research interests include wireless and wired data communications, localization systems, MIMO radars, and smart grids. He has served as an Area Editor for IEEE TRANSACTIONS ON COMMUNICATIONS and an Associate Editor for IEEE WIRELESS COMMUNICATIONS LETTERS and IEEE TRANSACTIONS ON WIRELESS COMMUNICATIONS.

Open Access funding provided by 'Università degli Studi di Modena e Reggio Emilia' within the CRUI CARE Agreement